AIAA JOURNAL
Vol. 31, No. 11, November 1993

# Length Scales and the Energy Balance for Turbulence Near a Free Surface

R. A. Handler,* T. F. Swean Jr.,† R. I. Leighton,† and J. D. Swearingen‡
*Naval Research Laboratory, Washington, D.C. 20375*

**The structure of turbulence near a free surface is examined by using results obtained from a direct simulation of flow between a no-slip wall and a shear free boundary, which serves as a model of a waveless free surface. An energy balance analysis shows that the pressure-strain term is the dominant producing term for the spanwise component of the turbulent kinetic energy. In addition, the dissipation rates for the horizontal components of the turbulence are reduced near the free surface, whereas the dissipation rate for the vertical component remains approximately constant. Two-point correlations, energy spectra, and length scales reveal important free surface induced effects. The length scales near the free surface are compared with the scales near the centerline of normal turbulent channel flow. This comparison reveals an increase by a factor of three in the streamwise length scales associated with the spanwise velocity fluctuations and an increase by a factor of two in the spanwise length scales for the streamwise velocity fluctuations. The length scales normal to the free surface are decreased for all velocity components. This indicates a more pancake-like eddy structure near the free surface compared with the structure near the centerline of a normal channel. The energy spectra show qualitative agreement with the Hunt-Graham model, though higher resolution calculations will be required to make more quantitative comparisons. The streaky structure in free surface bounded turbulent channel flow is noticeably more persistent than in normal turbulent channel flow. This is principally due to the attachment of streamwise oriented wall eddies to the free surface.**

## I. Introduction

TURBULENCE near a free surface differs fundamentally from its well studied counterpart, turbulence near a rigid no-slip boundary. Near a no-slip wall, the fluid motions are constrained by the boundary, and the turbulence production is large due to the existence of the mean shear. The simultaneous presence of both effects near a solid wall makes it difficult to determine the independent effects of each on the structure of turbulence. The wall places an inherent limit on the size of the turbulent eddies, and the mean shear may act to intensify the streamwise oriented eddies that are known to persist near the wall. At a free surface, however, turbulence production can be neglected because of the vanishing mean shear. As a consequence, the turbulence can only be affected by the constraint on vertical fluid motions imposed by the free surface. Note, however, that unlike flow near a no-slip boundary, the wall normal vorticity at the free surface may be nonzero. This result allows for the possibility that vortical structures may reconnect or attach themselves to the free surface.

In an effort to determine the structure of turbulence in the absence of mean shear, Uzkan and Reynolds[1] (UR) passed grid generated homogeneous turbulence over a wall that moved at the same streamwise velocity as the mean flow. They found that the streamwise turbulence intensity near the boundary did not peak as it does near a solid wall but instead decreased monotonically from its freestream value to zero at the boundary. Later, Thomas and Hancock[2] (TH) performed a similar experiment at a Reynolds number about 20 times greater than that of UR and found that the intensity of the streamwise component increases as the boundary is approached. The discrepancy between these two results was explained satisfactorily by Hunt and Graham[3] (HG) who proposed a two-layer model for the interaction. At high turbulent Reynolds numbers there exists a thin viscous layer near the wall embedded in a larger source layer. The source layer should be roughly the size of the integral length scale of the freestream turbulence and exists essentially because of the no mass flux condition at the boundary. Their theory predicts a redistribution of turbulent energy in the source layer from the vertical component of velocity to the streamwise and spanwise components. The UR result was easily explained because, at the low Reynolds number of their experiment, the viscous layer dominated the region near the surface, and the turbulence was accordingly damped. At the higher Reynolds number of the TH experiment, the source layer dominated, and the redistribution of the turbulence was confirmed according to the HG model. Many of these results were later confirmed by the large eddy simulations of Biringen and Reynolds.[4] Recently, Brumley and Jirka[5] (BJ) presented results for experiments in which homogeneous turbulence interacted with a free surface. Their results agreed reasonably well with a modified form of the HG model.

The simulations performed here were designed to represent as closely as possible the physics of free surface/turbulence interaction in which the effects of surface waves can be safely neglected. For this purpose, fully developed turbulence between a solid wall and a free surface is simulated. The physical processes represented by these simulations differ in some important respects from processes involved in the physical experiments noted earlier. First, in these simulations, no viscous layer can develop since $u_1$ and $u_3$, the fluctuating streamwise and spanwise velocity components, are not forced to zero as in the UR and TH experiments. Secondly, the turbulence impinging on the free surface is not isotropic. The no-slip wall is acting as a source of anisotropic turbulence, which is then convected toward the free surface. These simulations also allow for an examination of the influence of the free surface on the near wall turbulent structure, which will be discussed in detail in Sec. VI.

Presented as Paper 91-1775 at the AIAA 22nd Fluid Dynamics, Plasmadynamics, and Lasers Conference, Honolulu, HI, June 24–26, 1991; received Sept. 30, 1991; revision received Jan. 29, 1993; accepted for publication Feb. 8, 1993. 

*Research Mechanical Engineer, Remote Sensing Division.
†Research Mechanical Engineer, Remote Sensing Division. Member AIAA.
‡Research Mechanical Engineer; permanent address: Department of Mechanical Engineering, University of Kansas, Lawrence, KS, 66045. Member AIAA.

## II. Direct Numerical Simulation

The incompressible, three-dimensional Navier-Stokes equations were solved for initial and boundary conditions approximating a turbulent open-channel flow at a Reynolds number $Re_h$ based on the channel height $h$ and the mean velocity at the free surface $\overline{U}_s$ of 2340. The notations $x_1$, $x_2$, and $x_3$ will be used to denote the streamwise, wall-normal, and spanwise coordinates, respectively. The governing equations were recast in the manner suggested by Orszag and Patera[6] and implemented by Kim et al.[7] The final equation system, in which the pressure has been eliminated, consists of a fourth-order equation for the vertical velocity $U_2$

$$\left(\frac{\partial \nabla^2}{\partial t} - \frac{\nabla^4}{Re_h}\right)U_2 = \left(\frac{\partial^2}{\partial x_1^2} + \frac{\partial^2}{\partial x_3^2}\right)(U \times \Omega)_2 - \frac{\partial}{\partial x_2}\left[\frac{\partial}{\partial x_1}(U \times \Omega)_1 + \frac{\partial}{\partial x_3}(U \times \Omega)_3\right] \tag{1}$$

and a second-order equation for the vertical vorticity $\Omega_2$:

$$\left(\frac{\partial}{\partial t} - \frac{\nabla^2}{Re_h}\right)\Omega_2 = \frac{\partial}{\partial x_3}(U \times \Omega) - \frac{\partial}{\partial x_1}(U \times \Omega)_3 \tag{2}$$

where all variables are made nondimensional by $h$ and the initial value of $\overline{U}_s$. Here, the instantaneous velocity vector is given by $U$, and the instantaneous vorticity vector is defined by $\Omega = (\nabla \times U)$. Following the solution of Eqs. 1 and 2, the streamwise and spanwise velocity components $U_1$ and $U_3$ are recovered from the incompressibility condition.

The equations of motion are solved in Fourier-Chebyshev space, where Fourier modes are employed in the horizontal plane and Chebyshev modes in the wall-normal direction. The calculations were performed on a $64 \times 65 \times 48$ grid in $x_1$, $x_2$, and $x_3$, respectively. With the geometry scaled by the channel height, the streamwise, vertical, and spanwise dimensions of the channel are $4\pi$, 1, and $3\pi/2$, respectively. In terms of the viscous parameters consisting of the friction velocity $u_\tau$, and the kinematic viscosity $\nu = \mu/\rho$, where $\mu$ is the viscosity and $\rho$ is the density, the domain is $1684\ell^* \times 134\ell^* \times 632\ell^*$, where $\ell^* = \nu/u_\tau$. In these simulations the driving pressure gradient is held constant so that the relevant Reynolds number is $R^* = u^*h/\nu$. In the free surface turbulence calculation, $R^*$ achieves a steady-state value of 134. To facilitate substantive comparisons with the wall-bounded turbulence problem, a companion calculation for a closed-channel flow (i.e., a domain bounded by two no-slip walls), is used. For reasons of economy, this calculation was performed at a lower Reynolds number, $R^* = 125$, and at half the wall-normal resolution of the free surface simulation.

The boundary conditions are periodic on all dependent variables in the streamwise and spanwise directions. No-slip conditions are used at the bottom of the channel, and the free surface is approximated by using shear free boundary conditions. The shear free condition is an approximation to the exact free surface condition that is valid at low Froude number for a surface free of any contaminants. It can be estimated a posteriori, by using the parameters of our simulation and the experimental results of Komori et al.,[8] that the surface deflections are expected to be approximately $1.6 \times 10^{-4}m$ $(0.004h)$ and are clearly negligible. The boundary conditions at the solid wall ($x_2 = 0$) and the free surface ($x_2 = 1$) are given explicitly by

$$U_1 = U_2 = U_3 = 0; \qquad x_2 = 0 \tag{3}$$

and

$$\frac{\partial U_1}{\partial x_2} = \frac{\partial U_3}{\partial x_2} = U_2 = 0; \qquad x_2 = 1 \tag{4}$$

A simulation with identical boundary conditions was recently performed by Lam and Banerjee,[9] who used it to investigate near-wall streak formation.

The computer code used in the simulation was designed and developed to run on the Cray X-MP/24 at the Naval Research Laboratory. Approximately $10^{-5}$ s per time step per grid point were required for the simulation. Once the turbulence has achieved a statistically steady state, independent realizations of the instantaneous velocity field are saved during a time interval of approximately $4000t^*$, where $t^* = \nu/u_\tau^2$. Statistics are obtained by averaging in the streamwise and spanwise directions as well as over all realizations.

## III. Turbulent Energy Balance and Other Statistics Near the Free Surface

The unique features of turbulence near a free surface are revealed by examining the profiles of the turbulent kinetic energy, dissipation rate, and other basic statistics of the turbulence. The mean velocity $\overline{U}^+ = \overline{U}/u_\tau$ for open-channel flow is shown in Fig. 1 along with the wall laws $\overline{U}^+ = x_2^+$ and $\overline{U}^+ = 2.5\ell n x_2^+ + 5.5$, where $x_2^+ = x_2/\ell^*$. A best fit of the present open-channel simulation data for the logarithmic region is $\overline{U}^+ = 2.4\ \ell n x_2^+ + 5.6$. The slope of the logarithmic region in open-channel flow is evidently smaller than for a closed channel but this smaller slope is consistent with the value of 2.43 found by Nezu and Rodi[10] for open-channel flows over the Reynolds number range $439 \le R^* \le 6139$. The intercept is near the upper bound $(5.29 \pm 0.47)$ found in their experiments and is probably a low Reynolds number effect.[11] The notable difference between the velocity data in Fig. 1 and closed-channel behavior is the absence of a clearly defined wake region in the outer flow. In open-channel turbulence the log law is maintained until very close to the free surface where the velocity adjusts to the vanishing gradient conditions.

In Fig. 2 the results for the normalized turbulence kinetic energy $k = \frac{1}{2}(\overline{u_1^2} + \overline{u_2^2} + \overline{u_3^2})$ and the Reynolds shear stress $\overline{u_1 u_2}$ are shown. According to the boundary conditions given by Eqs. (3) and (4) the velocity components and pressure can be expanded about the free surface as

$$\begin{aligned} u_1 &= a_1 + c_1 x_2^2 + O(x_2^3) \\ u_2 &= b_2 x_2 + d_2 x_2^3 + O(x_2^4) \\ u_3 &= a_3 + c_3 x_2^2 + O(x_2^3) \\ p &= a_p + c_p x_2^2 + O(x_2^3) \end{aligned} \tag{5}$$

where $x_2$ is defined with the origin at the free surface. Use of these expansions and averaging results in $k = \frac{1}{2}(\overline{a_1^2} + \overline{a_3^2})$

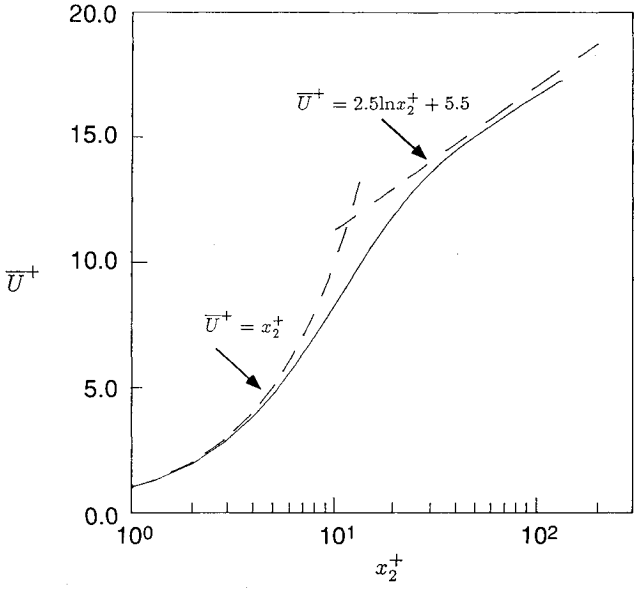


**Fig. 1 Mean velocity profiles. Open-channel simulation, ——; wall laws, — —.**

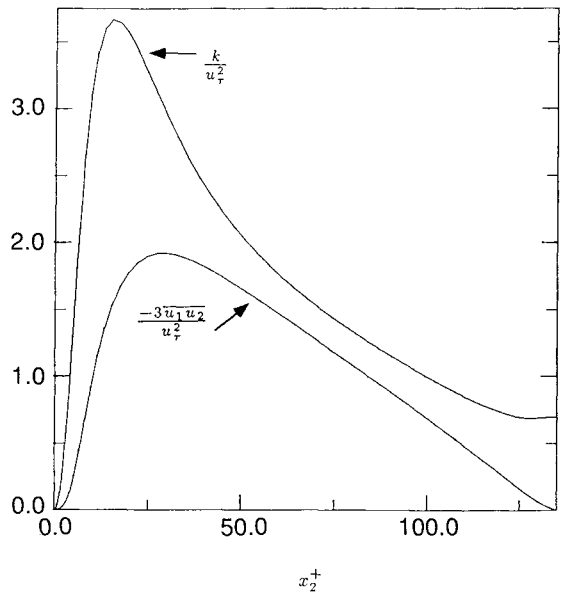


**Fig. 2 Turbulence kinetic energy and Reynolds stress profiles.**

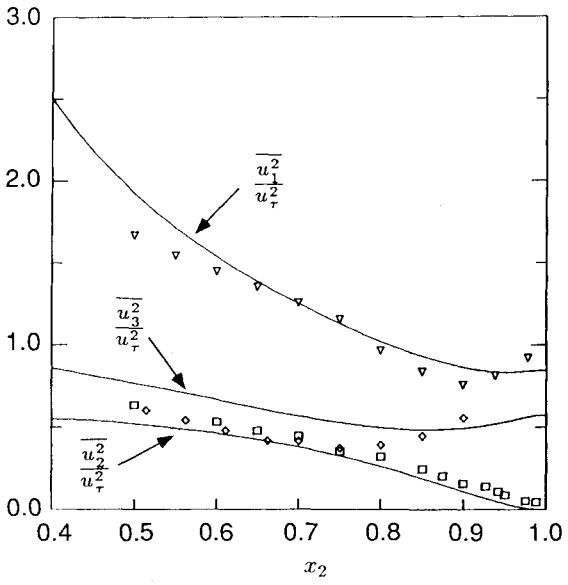


**Fig. 3 Normal stress profiles. Open-channel simulation, ——; experiments of Komori et al.,[8] ▽, $\overline{u_1^2}/u_\tau^2$; □, $\overline{u_2^2}/u_\tau^2$; and ◇, $\overline{u_3^2}/u_\tau^2$.**

$+ O(x_2^2)$ near the free surface and $\partial k/\partial x_2 = 0$ at the surface, which is evident in Fig. 2.

In Fig. 3, the three components of $k$ from the simulation are compared with the experimental results of Komori et al.,[8] which were obtained at $Re_h \approx 3100$. There is qualitative agreement between the experimental and numerical results. Both exhibit an increase in the horizontal components of the turbulence as the free surface is approached, and the increase is greatest for the spanwise component. The computed local minimum of the spanwise component occurs farther from the free surface compared with the streamwise component, which is also consistent with the experiments. This behavior is more easily recognizable in Fig. 4, which contains the distributions of the three components of the turbulence kinetic energy made nondimensional by the local value of $k$. The results from the closed-channel calculation are also shown in Fig. 4 for purposes of comparison. For the closed-channel calculation, $x_2 = 1$ corresponds to the channel centerline. It is evident that near the free surface ($x_2 > 0.7$) most of the energy from the vertical component is transferred to the spanwise component with only a small increase in the horizontal component. This result contrasts with the behavior of the various components of turbulence energy in the closed-channel simulation, where the relative interchange of energy appears to be primarily from the streamwise component of velocity to the vertical component in the region near the channel centerline. To understand this behavior, the energy and dissipation rate budgets have been examined.

For the flow under consideration, which is statistically steady and homogeneous in the spanwise and streamwise directions, the transport equations for the one-point velocity correlations are

$$\frac{D\overline{u_i u_j}}{Dt} = 0 = P_{ij} + \Pi_{ij} + T_{ij} + \Phi_{ij} + D_{ij} - \epsilon_{ij} \tag{6}$$

The symbols on the right-hand side of Eq. (6) denote the rates of production, pressure diffusion, turbulent transport, pressure strain, viscous diffusion, and dissipation, respectively. The explicit representations of these terms are

$$\begin{aligned}
P_{ij} &= -\overline{u_1 u_k}\frac{\partial \overline{U}_j}{\partial x_k} - \overline{u_j u_k}\frac{\partial \overline{U}_i}{\partial x_k} \\
\Pi_{ij} &= -\frac{1}{\rho}\left(\overline{\frac{\partial p u_j}{\partial x_i}} + \overline{\frac{\partial p u_i}{\partial x_j}}\right) \\
T_{ij} &= -\frac{\partial}{\partial x_k}\overline{u_i u_j u_k} \\
\Phi_{ij} &= \overline{\frac{p}{\rho}\left(\frac{\partial u_j}{\partial x_i} + \frac{\partial u_i}{\partial x_j}\right)} \\
D_{ij} &= \nu\frac{\partial^2 \overline{u_i u_j}}{\partial x_k \partial x_k} \\
\epsilon_{ij} &= 2\nu\overline{\frac{\partial u_i}{\partial x_k}\frac{\partial u_j}{\partial x_k}}
\end{aligned} \tag{7}$$

The equation obtained by taking half the trace of Eq. (6) is the equation for the turbulence kinetic energy $k$. The equation for the trace of the dissipation rate tensor, $\epsilon = (\epsilon_{11} + \epsilon_{22} + \epsilon_{33})/2$, is given by Hanjalić and Launder[12] as

$$\begin{aligned}
\frac{D\epsilon}{Dt} = 0 = &-2\nu\left(\overline{\frac{\partial u_i}{\partial x_\ell}\frac{\partial u_k}{\partial x_\ell}}\right)\frac{\partial \overline{U}_i}{\partial x_k} - 2\nu\left(\overline{\frac{\partial u_\ell}{\partial x_i}\frac{\partial u_\ell}{\partial x_k}}\right)\frac{\partial \overline{U}_i}{\partial x_k} \\
&- 2\nu\overline{u_k\frac{\partial u_i}{\partial x_\ell}}\frac{\partial^2 \overline{U}_i}{\partial x_k \partial x_\ell} - 2\nu\overline{\frac{\partial u_i}{\partial x_k}\frac{\partial u_i}{\partial x_\ell}\frac{\partial u_k}{\partial x_\ell}} \\
&- \frac{2\nu}{\rho}\frac{\partial}{\partial x_k}\left(\overline{\frac{\partial p}{\partial x_\ell}\frac{\partial u_k}{\partial x_\ell}}\right) - \nu\frac{\partial}{\partial x_k}\overline{u_k\left(\frac{\partial u_i}{\partial x_j}\frac{\partial u_i}{\partial x_j}\right)} \\
&+ \nu\frac{\partial^2 \epsilon}{\partial x_k^2} - 2\overline{\left(\nu\frac{\partial^2 u_i}{\partial x_k \partial x_\ell}\right)^2}
\end{aligned} \tag{8}$$

The first four terms are production terms ($P_\epsilon^1$ to $P_\epsilon^4$), and terms five through eight are pressure transport ($\Pi_\epsilon$), turbulent transport ($T_\epsilon$), viscous diffusion ($D_\epsilon$), and dissipation ($Y$), respectively.

The terms in the budget equations for the three normal stresses and the dissipation rate are shown in Figs. 5–8. All terms in Eqs. (7) and (8) have been normalized by $u_\tau^4/\nu$, and the budgets are displayed only for the upper half of the channel nearest the free surface. Figure 5 shows that away from the free surface all terms in the $\overline{u_1^2}$ budget have the same relative importance except $D_{11}$, the viscous diffusion. (Note that $\Pi_{11} = \Pi_{33} = 0$, because the flow is homogeneous in the horizontal plane.) As the free surface is approached, the production rate vanishes with the mean velocity gradient. Analysis of the results near the no-slip boundary, not shown here, indi-

cates that the viscous terms balance the turbulence transport and the pressure-strain terms, the latter becoming a slight positive contributor to the budget very near the wall. The $\overline{u_2^2}$ balance shown in Fig. 6 is relatively more complex than that for $\overline{u_1^2}$. For this component, the magnitude of the budget terms near the free surface is only reduced by about one-half compared with their values near a solid wall. Near the free surface, the asymptotic behavior of the various terms can be determined by using Eq. (5) as

$$
\begin{aligned}
T_{22} &= -3\overline{b_2^3}x_2^2 + \cdots \\
\Pi_{22} &= -2\overline{a_p b_2} - 6(\overline{c_p b_2} + \overline{a_p d_2})x_2^2 + \cdots \\
\Phi_{22} &= 2\overline{a_p b_2} + 2(\overline{c_p b_2} + 3\overline{a_p d_2})x_2^2 + \cdots \\
D_{22} &= 2\overline{b_2 b_2} + 24\overline{b_2 d_2}x_2^2 + \cdots \\
\epsilon_{22} &= 2\overline{b_2 b_2} + 12\overline{b_2 d_2}x_2^2 + \cdots
\end{aligned}
\tag{9}
$$

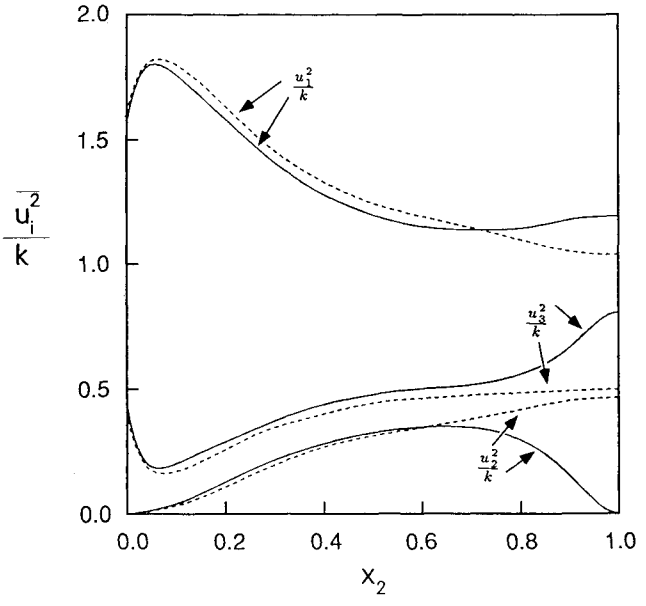


**Fig. 4 Normal stress profiles normalized by the local value of the turbulence kinetic energy. Open-channel simulation, ——; closed-channel simulation, — —.**

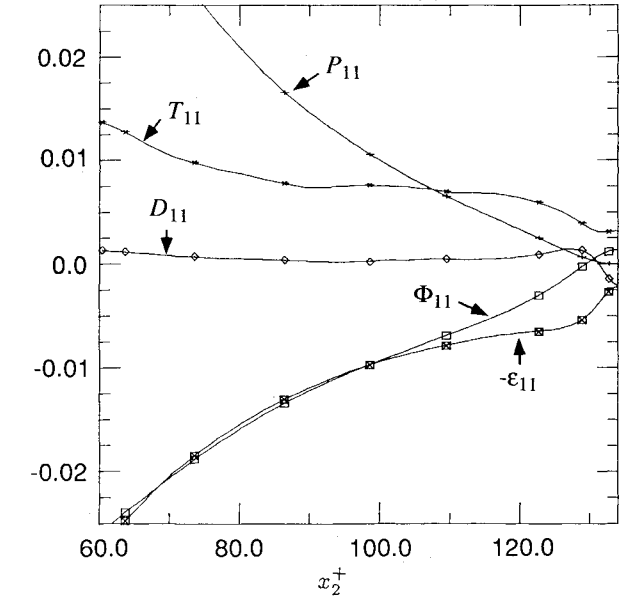


**Fig. 5 Distribution of the terms in the budget for $\overline{u_1^2}$ in the upper half of the channel.**

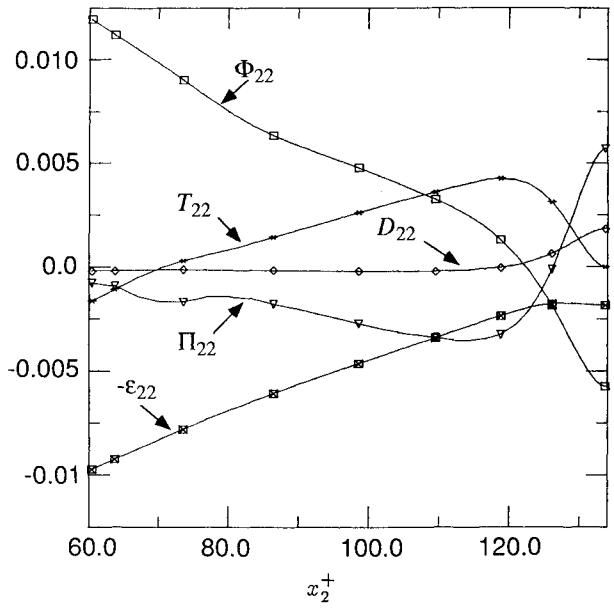


**Fig. 6 Distribution of the terms in the budget for $\overline{u_2^2}$ in the upper half of the channel.**

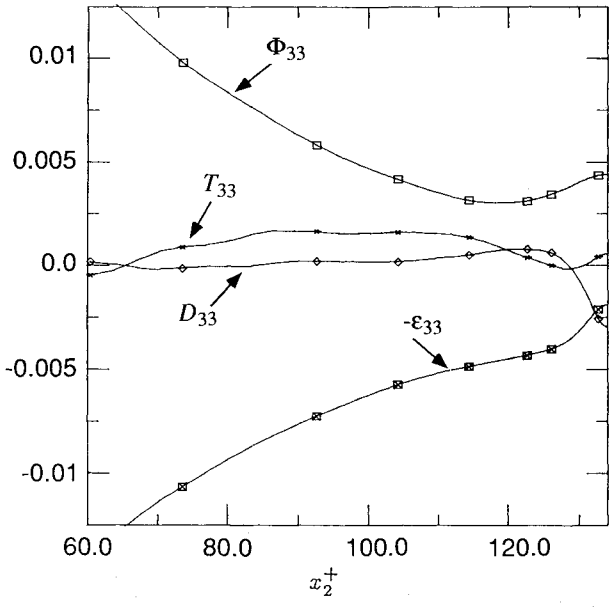


**Fig. 7 Distribution of the terms in the budget for $\overline{u_3^2}$ in the upper half of the channel.**

It is seen that at the free surface $\epsilon_{22}$ balances $D_{22}$, and the two pressure-velocity terms cancel. Note that the pressure-strain term has rapidly become a consuming term in the near surface region whereas it is a major producer in the budget equation farther from the free surface. This result is in contrast to the behavior shown in Fig. 7 for the $\overline{u_3^2}$ component. In this case $\Phi_{33}$ increases near the free surface and at the surface is considerably more of a source for $\overline{u_3^2}$ than $\Phi_{11}$ is for $u_1^2$. Similar observations have recently been made by Komori et al.[13] This behavior largely explains why the transverse component of kinetic energy (Fig. 4) is increased relatively more so than the streamwise component.

A curious feature contained in Figs. 5 and 7 is the behavior of $\epsilon_{11}$ and $\epsilon_{33}$ as the surface is approached. Near the free surface the dissipation rates exhibit a sharp drop in magnitude in the upper 5 to 10% of the channel. On the other hand, $\epsilon_{22}$ shows a very slight increase in magnitude and could well be approximated as constant in this region. This behavior is contrary to standard modeling assumptions near the free surface. Hossain and Rodi[14] and later Naot and Rodi[15] have

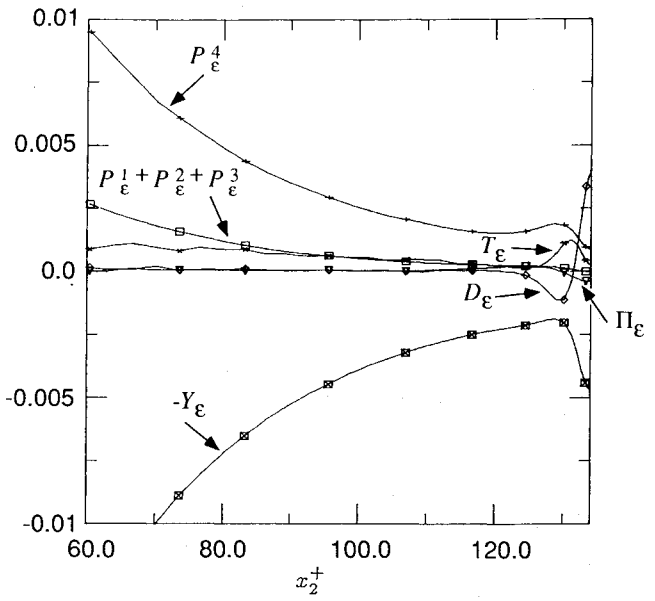


**Fig. 8 Distribution of the terms in the budget for the turbulence kinetic energy dissipation rate in the upper half of the channel.**

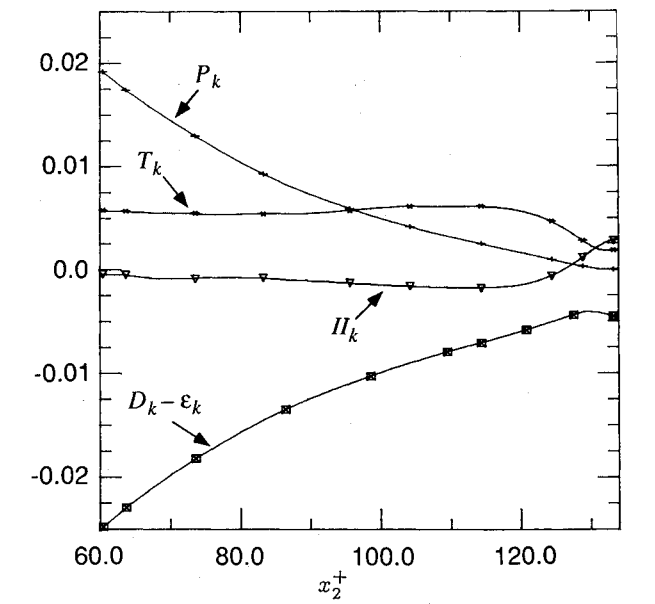


**Fig. 9 Distribution of the terms in the budget for the turbulence kinetic energy in the upper half of the channel.**

assumed that in most respects other than the vanishing of the surface-normal velocity component, the free surface behaves like a symmetry plane. The exception is the presumed behavior of the dissipation rate for turbulence kinetic energy, which is expected to increase near the surface. This is based on the assumption that the characteristic length scale of the turbulence ($L \propto k^{3/2}/\epsilon$) is reduced by the presence of the boundary. The turbulent length scales in fact do not become zero because they reflect the fluctuating motion in all three directions, and the horizontal extent of the eddies is not restricted. In fact, in Sec. V it is shown that the macroscales in the horizontal plane actually increase near the free surface.

The terms in the budget equation for the dissipation rate are shown in Fig. 8. In the upper portion of the channel, the first three production terms in Eq. (8) are small and have been lumped together as shown. Until very near the free surface the production by turbulence $P_\epsilon^4$ largely balances the dissipation term. Very near the surface the dominant terms are the viscous diffusion and the dissipation, each exhibiting very large gradients of opposite sign near the boundary. Reconsidering Figs. 5 and 7, it is seen that also in these cases the rapid variation in the dissipation term appears to be at least partially offset by the variation in the diffusion term. It should be remembered that $\epsilon_{ii}$ (or $\epsilon$) is not the actual dissipation of turbulent energy for inhomogeneous flows, although it does approximate the total dissipation for high Reynolds number flows. The particular terms $D_{ii}$ and $\epsilon_{ii}$ arise from the combination of the actual dissipation rate with the rate of work done by viscous shear stresses.[16] In flows far from solid walls the viscous diffusion is generally neglected, and as such the modeled dissipation rate implicitly models the work term.

The balance of turbulence kinetic energy obtained from the trace of Eq. (6) is shown in Fig. 9. The viscous terms have been added, and together they balance the transport terms at the free surface. It is seen that the total viscous term varies only slightly near the free surface and might be easier to model than the individual viscous terms. It is beyond the scope of the current work, however, to pursue turbulence modeling near the free surface, which has been pursued elsewhere.[17] Next, the structural aspects of the turbulence are investigated by examining the two-point correlations, energy spectra, and length scale profiles near the free surface.

## IV. Two-Point Correlations and Energy Spectra

The structure of the turbulence near the free surface is revealed in some detail by examining the two-point correlations and energy spectra at different depths below the surface. The two-point correlation function $R_{ij}$ is defined by

$$R_{ij}(\Delta x_1, \Delta x_3, x_2, x_2') = \frac{\overline{u_i(x_1, x_3, x_2)u_j(x_1', x_3', x_2')}}{\sqrt{\overline{u_i^2}\,\overline{u_j^2}}} \tag{10}$$

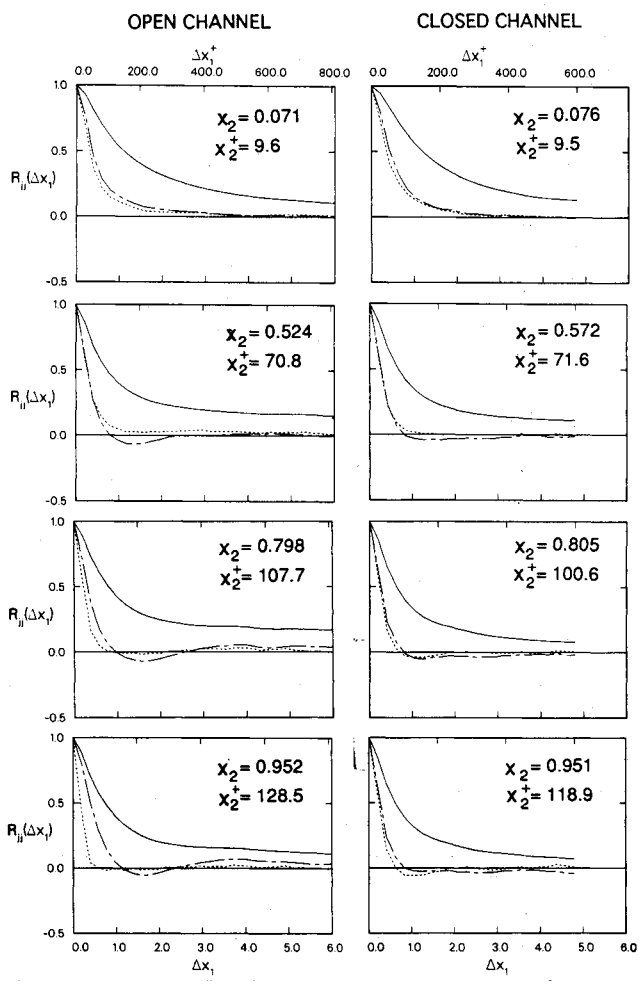


**Fig. 10 Streamwise two-point correlations. $R_{11}$, ——; $R_{22}$, - - -; $R_{33}$, — - —.**

Here, only the properties of $R_{ij}$ for which $x_2 = x_2'$ and $i = j$ are described. These correlations were computed by averaging over all flow realizations and all flow symmetries.[18]

The streamwise correlations for open- and closed-channel flows are compared at several $x_2^+ = u_\tau x_2/\nu$ locations in Fig. 10. Note that in each figure a secondary axis is given showing the separation lengths in terms of wall variables. In the region close to the bottom solid wall ($0 < x_2 < 0.5$; $0 < x_2^+ < 68$) the streamwise correlations are virtually identical for all three velocity components. As an example, note the similarity between the correlations at $x_2 = 0.071$ for open-channel turbulence with those for closed-channel turbulence at $x_2 = 0.076$. The only notable difference is a somewhat longer streamwise correlation length for $u_1$ in the open-channel case. At distances farther from the wall, however, the differences between the two flows become increasingly pronounced. As the free surface is approached, two trends are evident. First, the streamwise distance at which $R_{33}(\Delta x_1, 0, x_2)$ [subsequently denoted $R_{33}(\Delta x_1)$] attains its minimum value increases as the free surface is approached. For example, at $x_2 = 0.524$, the minimum occurs $\Delta x_1 \simeq 1.34$, and as the free surface is approached this increases to $\Delta x_1 \simeq 1.57$. For the closed-channel case, however, there is no discernible change in $R_{33}(\Delta x_1)$ as $x_2$ varies from 0.572 to the centerline. [A possible interpretation for the existence of a minimum in $R_{33}(\Delta x_1)$ is discussed in more detail in Sec. VI.] Secondly, for the open channel, the streamwise correlation length of the vertical component of velocity, which may be loosely defined by the first zero crossing, decreases significantly from $x_2 = 0.524$, where no zero crossing exists, to $x_2 = 0.952$, where it attains a value of about 0.75. In the closed-channel case this scale also decreases, but not nearly as rapidly as in open-channel turbulence, where there appears to

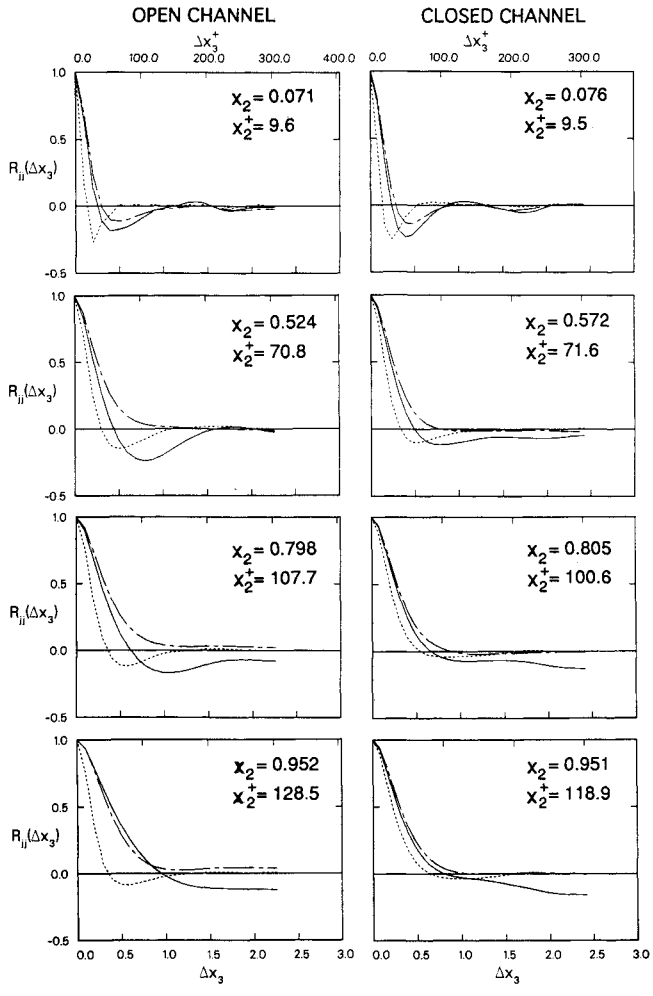


**Fig. 11 Spanwise two-point correlations.** $R_{11}$, ——; $R_{22}$, - - -; $R_{33}$, — • —.

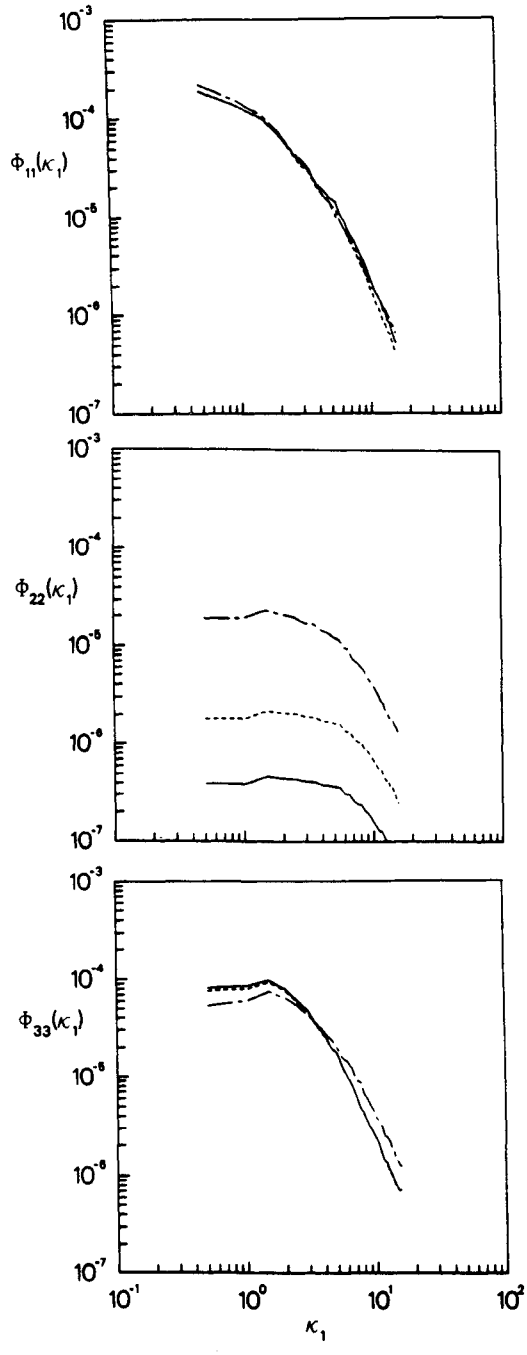


**Fig. 12 Velocity spectra near the free surface.** $x_2 = 0.978$, ——; $x_2 = 0.952$, - - -; $x_2 = 0.798$, — • —.

be a clearer separation between $R_{22}(\Delta x_1)$ and $R_{33}(\Delta x_1)$ near the free surface.

In Fig. 11 the corresponding results for the spanwise correlations $R_{jj}(\Delta x_3)$ are shown. As in the streamwise results, close to the wall there appear to be no significant differences between these flows. Farther from the wall ($x_2 \geq 0.5$), it is evident that the correlation length for $u_2$ in open-channel turbulence is significantly smaller compared with correlation lengths for the other velocity components. This behavior is not evident for the closed-channel case in this region. Again, as with the streamwise correlation results, there is a clear separation between $R_{22}(\Delta x_3)$ and $R_{33}(\Delta x_3)$ as the free surface is approached. One feature of note is the persistence of a local minimum in $R_{11}(\Delta x_3)$ in open-channel turbulence. From Fig. 11 it appears that this minimum, which is indicative of a periodic spanwise structure, continues to be evident out to $x_2 \approx 108l^*$. The significance of this observation is discussed in more detail in Sec. VI.

Energy spectra $\Phi_{ij}$ as a function of streamwise wave number $\kappa_1 = 2\pi n/L_1$, $0 \le n \le 32$, are shown in Fig. 12 for two surface-normal locations in close proximity to the free surface ($x_2 = 0.978$ and 0.952). A third energy spectrum at $x_2 = 0.798$, relatively far from the free surface, is also given in each plot as a reference condition because at this depth, free surface effects should not be significant. The spectra for the streamwise velocity component $\Phi_{11}$ show that very near the free surface, the energy at low wave numbers remains unchanged. However, for the intermediate band ($2 < \kappa_1 < 10$) a very small increase in energy is evident. There is no change in the spectrum at high wave numbers. From the $\Phi_{22}$ spectra it is quite evident that as the free surface is approached, the energy at low wave numbers decreases more rapidly than at high wave numbers. This result is consistent with the HG model predictions, though it should be noted that the model predicts that the $\Phi_{22}$ spectra obtained far from the free surface will merge with the spectra near the free surface. This merger will occur at a wave number of order $2\pi/\Delta x_2$, where $\Delta x_2$ is the vertical distance from the free surface, and is effectively caused by the cutting off of eddies smaller than $\Delta x_2$ by the presence of the surface. In these calculations, however, the minimum resolvable streamwise length scale dictated by the grid spacing is $(4\pi/64) = 0.196$, which is in fact of the same order as the source layer. It is evident that higher resolution is required to resolve these effects. Nevertheless, the basic structure of $\Phi_{22}$ is suggestive of this kind of wave number cutoff behavior. The spectrum $\Phi_{33}$ shows some increase at low wave numbers but virtually no change for $\kappa_1 > 3$.

## V. Macro and Microscales near the Free Surface

### A. Length Scales in the Homogeneous Directions

The correlations $R_{ij}$ can be used to obtain both the macroscales and microscales of the turbulence. These measures give not only quantitative information about the turbulent eddy sizes but also a qualitative picture of how the free surface modifies the turbulent structure. A measure of the largest structures in the flow, sometimes referred to as the energy containing eddies, are determined by computing the turbulent macroscale.[16] The macroscale $\Lambda_{ij}$ corresponding to velocity component $u_j$ in direction $x_i$ is defined by

$$\Lambda_{ij} = \int_0^\infty R_{jj}(\Delta x_i)\, dx_i \tag{11}$$

The microscale, though not the smallest length scale in the flow, can be thought of as an average length within which most of the energy dissipation occurs. In high Reynolds number homogeneous turbulence there is a large separation between these two scales, but in the current computations this separation is not large principally due to the low Reynolds number of the turbulence and its strong anisotropy. The microscale $\lambda_{ij}$ is defined by

$$\lambda_{ij}^2 = -2 \Big/ \left. \frac{\partial^2 R_{jj}(\Delta x_i)}{\partial^2 x_i} \right|_{x_i = 0} \tag{12}$$

If the turbulence is homogeneous in direction $x_i$, then it can be shown that an equivalent definition is

$$\lambda_{ij}^2 = \overline{u_j^2} \Big/ \overline{\left(\frac{\partial u_j}{\partial x_i}\right)^2} \tag{13}$$

The microscales computed using both definitions yielded identical results. Note that in some circumstances, particularly for the streamwise velocity component, the correlation function $R_{jj}(\Delta x_1)$ does not decay sufficiently at the end of the computational domain, so that the macroscale given by Eq. (11) may underestimate the true eddy size. Also, since quasiperiodic structures exist close to the wall with their periodicity primarily in the spanwise direction, $R_{jj}(\Delta x_3)$ can be negative. These negative values have the effect of producing a macroscale that underestimates the length of the largest eddy structures near the wall.

The results of the calculation of the streamwise macroscale $\Lambda_{1j}$ and the spanwise macroscale $\Lambda_{3j}$ for both the open- and closed-channel cases are shown in Fig. 13. Recall that in these plots the solid wall is at $x_2 = 0$, and the free surface (or centerline) is at $x_2 = 1$. The scales are nominally given in terms of the channel height, and conversion to wall variables can be obtained by multiplying by $R^* = 135$ in the open-channel case and $R^* = 125$ for the closed-channel case. For the streamwise macroscales, significant differences between these two cases are apparent in the rather large region $0.4 < x_2 < 1.0$. Here, the most notable observation is that $\Lambda_{13}$, the streamwise macroscale for the spanwise velocity component, increases by a factor of approximately three from $\approx 0.19$ at the centerline of the closed channel to $\approx 0.60$ at the free surface. The streamwise macroscale for the streamwise velocity component $\Lambda_{11}$ differs only slightly at the free surface from its value at the centerline of the closed channel. However, there is a very noticeable peak in $\Lambda_{11}$ near the free surface, which is not evident near the centerline of the closed channel. The free surface effects on the spanwise macroscale $\Lambda_{3j}$ are confined to the region $(0.8 < x_2 < 1.0)$. Substantial differences are again observed between the values attained at the free surface relative to those at the closed-channel centerline. The principal difference is a noticeable increase by a factor of about two for the streamwise velocity scale $\Lambda_{31}$. The vertical velocity scale $\Lambda_{32}$ shows a decrease by roughly a factor of two as well.

Trends similar to those found for the macroscales in Fig. 13 are apparent for the microscales $\lambda_{ij}$ shown in Fig. 14. The streamwise scale for the spanwise velocity $\lambda_{13}$ is larger at the free surface compared with its value at the closed-channel centerline (0.40 vs 0.29). The scale $\lambda_{12}$ shows a small but clearly evident decrease (0.21 vs 0.27). The trends for $\lambda_{3j}$ are also quite similar to those for the corresponding macroscale results with the salient feature being an increase in $\lambda_{31}$ near the free surface.

### B. Length Scales in the Inhomogeneous Direction and Summary

It is convenient to define a vertical macroscale $\Lambda_{2j}$ as follows:

$$\Lambda_{2j}(x_2) = \int_0^1 R_{jj}(0, 0, x_2, x_2')\, dx_2' \tag{14}$$

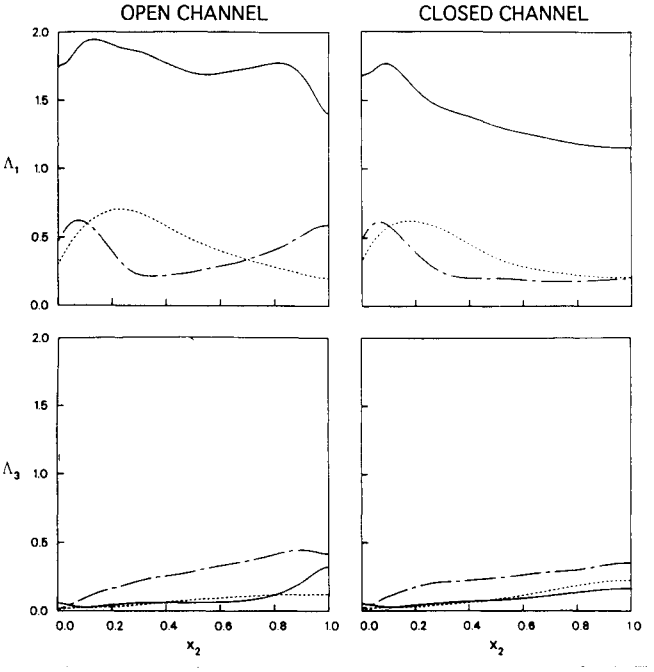


**Fig. 13 Macroscales in the streamwise and spanwise directions for both open- and closed-channel simulations. Streamwise velocity, ——; wall-normal velocity, - - -; spanwise velocity, — - —.**

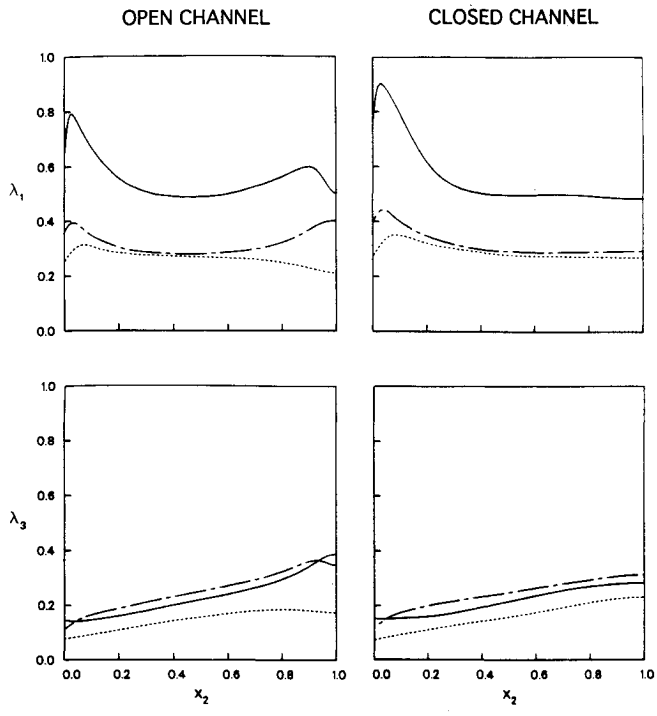


**Fig. 14 Microscales in the streamwise and spanwise directions for both open- and closed-channel simulations. Streamwise velocity, ——; wall-normal velocity, - - -; spanwise velocity, — - —.**

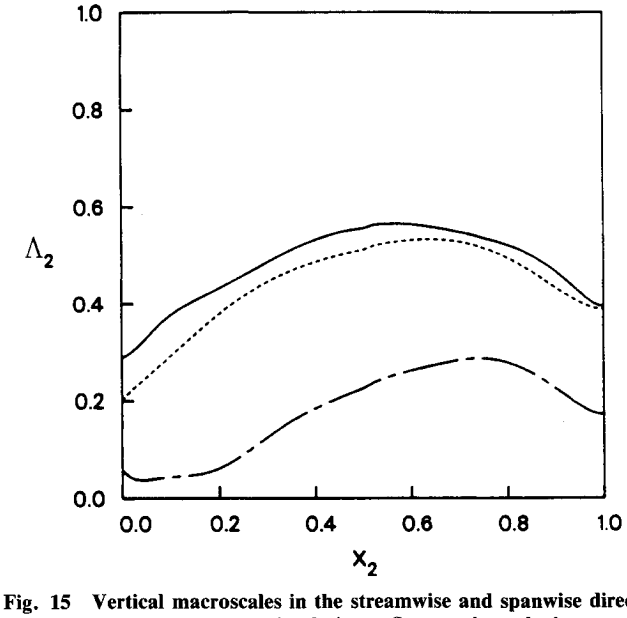


**Fig. 15 Vertical macroscales in the streamwise and spanwise directions for the open-channel simulations. Streamwise velocity, ——; wall-normal velocity, - - -; spanwise velocity, — - —.**

At a given vertical location $x_2$, $\Lambda_2$ gives a measure of the vertical size of a typical eddy that can exist at that depth. These results are shown in Fig. 15. It is evident that $\Lambda_{21}$ and $\Lambda_{22}$ increase continuously from the solid wall until $x_2 \simeq 0.6$, where free surface effects become evident as both length scales decrease. The $\Lambda_{23}$ macroscale results may not be easily interpreted near the solid wall since $R_{33}(x_2, x_2')$ becomes negative there, presumably due to the counter-rotating vortex structure typically associated with the wall layer. Near the free surface, however, $R_{33}(x_2, x_2')$ is strictly positive so that the interpretation of $\Lambda_{23}$ as a length scale is more meaningful. As with the other two vertical macroscale components, $\Lambda_{23}$ decreases noticeably as the free surface is approached. These results generally tend to confirm the HG model, which predicts a strong truncation of the vertical extent of a typical eddy near the free surface.

The length scale results are particularly useful in understanding the change in shape of a typical eddy as it interacts with the free surface. These results show clearly that the free surface acts quite differently from a simple symmetry plane, as represented by the channel centerline, principally due to the damping of the boundary normal velocity component. In this regard, the turbulence at the free surface is associated with larger spanwise scales associated with the streamwise velocity component; generally smaller streamwise and spanwise scales for the wall normal velocity component; and larger streamwise length scales associated with the spanwise velocity component. Additionally, the vertical macroscales ($\Lambda_{2j}$) associated with all three velocity components decrease on approach to the free surface. This presents a reasonably clear picture of eddies that flatten out or become pancake-like as they undergo a reduction in their vertical extent and an increase in their streamwise and spanwise extent by factors of three and two, respectively. This result is certainly in agreement with one's intuitive expectation of the effect of the free surface on an impinging eddy. It does not seem possible to make a quantitative comparison of these results with the HG model in its present form, because their model does not account for the strong anisotropy of the open-channel flow studied here. Obviously, defining a farfield integral length scale in this flow is difficult compared with homogeneous turbulence, where the integral length scale is easily defined and measured far from the free surface.

## VI. Streak Spacing

In Sec. IV the persistence of a periodic spanwise structure at relatively large distances away from the wall was noted for open-channel turbulence. These streamwise-elongated structures, commonly referred to as wall-layer streaks, appear in flow visualization studies as regions of low-speed fluid close to the wall. Though some controversy remains about the significance of the streaks, increasing evidence appears to show that they are indicators of quasistreamwise vortices.[19,20] These vortices are thought to play a role in the production of new turbulence and in Reynolds stress production. They were first observed experimentally by Hama (see Corrsin[21]) and later studied in more detail by Kline et al.[22] These visualization studies showed that the streaks were typically observed below $x_2^+ = 30$ and that they occurred randomly in space and time. The average spanwise spacing between the streaks $\overline{\lambda}^+$ is found to be approximately 100 and is essentially independent of

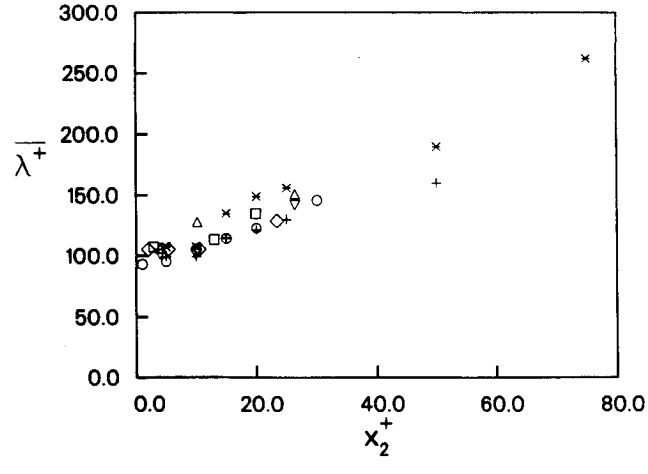


**Fig. 16 Variation of the mean spanwise streak spacing with wall-normal distance. Present study: *, open channel, $R^* = 135$; +, closed channel, $R^* = 125$. Smith and Metzler[24]: ○, boundary layer experiment. Schraub and Kline[25]: □, boundary layer experiment. Nakagawa and Nezu[23]: open-channel experiment, ▽, $R^* = 248$; △, $R^* = 378$. Kim, Moin, and Moser[7]: ◇, closed-channel simulation, $R^* = 180$.**

Reynolds number.[22] The experimental results reported by Nakagawa and Nezu[23] for open-channel flow indicate that the mean streak spacing increases with distance from the wall and ultimately approaches a value of $\overline{\lambda}^+ \approx 2x_2^+$ for $x_2^+ \geq 50$. This led them to speculate that the increase in length scale resulted from a coalescence (similar to the pairing interaction observed in free shear flows) of neighboring low-speed streaks as the distance from the wall increased. However, note that for the locations above $x_2^+ > 30$ the spanwise length scale they observe is very weak and may not necessarily correspond to well-defined streaks.

More recently, Smith and Metzler,[24] in agreement with the findings of Nakagawa and Nezu, found that the average spanwise wavelength increased from 93 at $x_2^* = 1$ to 146 at $x_2^+ = 30$. They noted, however, that beyond $x_2^+ = 30$ the streaks were not sufficiently well defined to warrant making streak counts, and they suggest that $x_2^+ \approx 40$ is the upper limit for which extended regions of low-speed fluid continue to exist. Also in agreement with Nakagawa and Nezu, they found that streak coalescence in the region $10 \leq x_2^+ \leq 30$ contributed to the increasingly disrupted streak pattern and overall increase in the spanwise length scale with distance from the wall. They noted that because the most active merging occurs in the region of maximum turbulent energy production, this merging process may very well be important to the turbulence production cycle. The observation of wall-layer streaks has not been confined strictly to experimental studies; various numerical simulations appear to very satisfactorily capture the wall-layer dynamics.[7]

In Fig. 16 the dependence of the streak spacing on $x_2^+$ is presented for both open- and closed-channel flows along with various experimental results and other numerical results. Here the streak spacing is defined as twice the spanwise distance at which $R_{11}(\Delta x_3)$ reaches a minimum. The results indicate clearly that for $x_2^+ < 12$, there is excellent agreement from all sources that $\overline{\lambda}^+ \simeq 100$. The streak spacing in the open-channel case shows a jump from about 105 at $x_2^+ = 12$ to about 130 at $x_2^+ = 15$. Farther from the wall, the open-channel streak spacing increases at a rate that is roughly the same as in the closed channel but always remains larger. One can infer from Fig. 16 that at $x_2^+ \simeq 65$, $\overline{\lambda}^+$ for the open-channel case is roughly twice its value at $x_2^+ \simeq 12$. Also clear is that, unlike the closed-channel case where the streak spacing is apparently only clearly defined out to $x_2^+ \simeq 50$, in the open channel the spacing can be defined out to $x_2^+ \simeq 80$. This is in fact within the logarithmic layer of the streamwise velocity profile. The streaky structure in open-channel turbulence is both larger in scale and persists farther from the wall when compared with closed-channel turbulence.

Though the reasons for these differences are far from evident, a few speculations are now offered to explain this behavior. The only obvious difference between these two flows is the boundary condition imposed on the upper surface. Because the shear free boundary suppresses the production of new turbulence, we can envision that this must in turn suppress the ejection of low-momentum fluid that would otherwise occur if the boundary were rigid (i.e., no-slip boundary conditions). The suppression of these ejections from the top boundary (free surface) toward the bottom boundary (solid wall) may be responsible for slowing down the production of turbulence by lowering the probability of shear layer formation in the region of the solid wall. Thus, the larger, more coherent streaks near the wall in open-channel turbulence may be due to the suppression of turbulence production at the free surface. Furthermore, in boundary-layer flow the entrainment of outer-irrotational fluid may act like ejections from the upper wall of a channel. In this sense, boundary-layer flow may be more like closed-channel flow than open-channel flow. These results suggest that the outer flow does have an effect on the wall region at least at these low Reynolds numbers.

An alternate but not exclusive explanation for the observed persistence of the streaky structure is the existence of stable vortical structures in open-channel turbulence. The vortex loops, originating in the near-wall and buffer regions of the flow, have been observed in other wall-bounded flows and originate in the region of strong mean shear near the wall. In open-channel turbulence, these structures, which are presumably generated as they are in other wall-bounded flows, move away from the solid wall toward the opposing shear free boundary. In the closed-channel case, these migrating structures would be subject to velocity fluctuations originating at the opposing wall. As mentioned earlier, the shear free boundary does not maintain a mean shear or aid in the production of random velocity fluctuations. Without the impeding velocity fluctuations, and assuming the vortex loop is sufficiently strong, it will interact and reconnect with the free surface. After the reconnection has occurred, the vortex loop exhibits a behavior very different from its closed-channel counterpart. In the closed case, the loop is buffeted by the flow and rapidly loses its coherence. In the open-channel case, however, the vortex structure becomes quite stable because it is unable to break free of the upper surface. In addition, the mean velocity strain maintains its strength. These vortex structures are observed to both strengthen and disappear, but they are observed to exist for hundreds of viscous time units. It was noted previously (Fig. 10) that the correlation $R_{33}(\Delta x_1)$ possesses a minimum that persists very close to the free surface. The existence of this minimum is entirely consistent with the surface-normal vorticity of these attached vortical structures. More details about the reconnection process can be found in Leighton et al.[26]

Evidence for the existence of these attached structures is given in Fig. 17. In Fig. 17a the flow on the free surface is visualized by advancing in time an array of particles released on the free surface. The velocity field used here is frozen in time, with the mean velocity removed. The particles converge into tight spirals that identify the vortices attached to the free surface. Although these particle paths would not be the paths observed in an experiment, because they have been obtained from a frozen field, a qualitative understanding of the surface flow is possible. The vortex structure associated with the spiral within the outlined rectangle of Fig. 17a is visualized in Fig. 17b. The surface visualized is that of constant vorticity magnitude equal to about 0.8. For comparison, the peak vorticity on the shear free surface take on values between 2 and 3. The structure is attached to the upper boundary at the upper left of

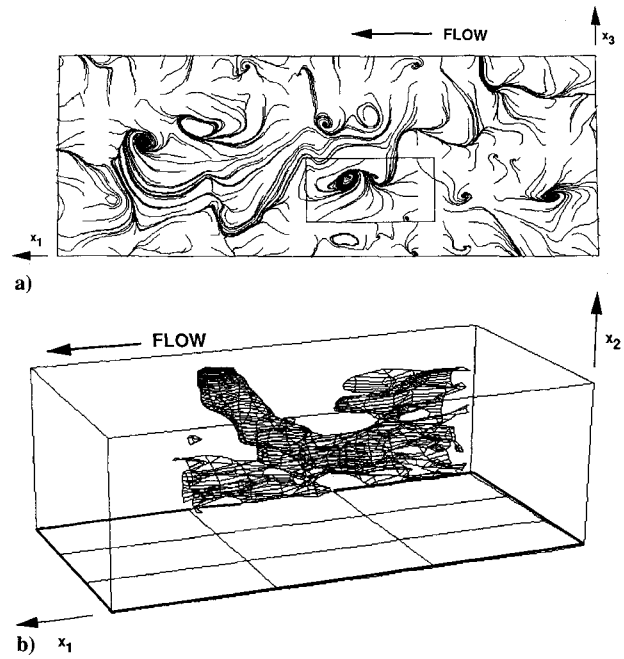


**Fig. 17 Attached vortex structures in open-channel flow: a) particle paths on free surface convected by a frozen velocity field and b) vortex structure associated with converging spiral in the small rectangle in a).**

the figure and extends toward the lower right. For clarity, the vorticity in the bottom 20% of the channel is not shown. Both an internal straining motion due to an internal pressure gradient and external strain due to the mean velocity field contribute to the maintenance of the attached vortex. The robust attached vortices and the associated shear layers are conjectured to be the mechanism responsible for the detectability of low-speed streaks at distances from the wall as large as $x_2^+ \simeq 80$.

## VII. Conclusions

The structure of turbulence near a free surface has been studied using the results of a direct simulation. The simulation results indicate that there is preferential redistribution of turbulence energy to the spanwise velocity component as the vertical component is damped near the free surface. This result is in accordance with the limited experimental observations. The budget equations show that the pressure-strain term is a key contributor to this behavior. In addition, the isotropic part of the dissipation of turbulent energy decreases rapidly very near the free surface, a result contrary to current modeling assumptions. An examination of the turbulent macroscales and microscales reveals a significant flattening of a typical eddy near the free surface compared with the structures that exist at the centerline of closed-channel turbulence. This flattening is evidenced by a notably larger streamwise scale associated with the spanwise velocity component and a commensurately larger spanwise scale of the streamwise velocity component. Additionally, the vertical length scales for all three velocity components are smaller than the companion closed-channel values. A direct quantitative comparison of these results with the HG model is not possible because the model does not currently account for the strong anisotropy of the turbulence present in this flow. Some features of the energy spectra are in qualitative agreement with the HG model though resolution effects and anisotropy limit direct qualitative comparison.

An interesting phenomenon revealed by the current study is the increase in size and persistence of the spanwise periodic structure near the wall. In open-channel turbulence this structure is larger in scale and penetrates farther into the flow than in closed-channel turbulent flow. The origin of this effect is not clear, but one possible explanation is that the free surface suppresses interactions that would normally occur between the no-slip boundaries of channel flow. The lack of an opposing boundary results in the existence of the log-layer until very near the free surface and in the existence and maintenance of vortex structures extending from the wall region to the free surface. Visualizations indicate that streamwise-oriented vortices can attach themselves to the free surface and appear to be remarkably stable in this configuration. This observation lends support to the possibility that the outer flow has a significant effect on wall-layer structure. In future work, a quantitative comparison of these results with a modified form of the HG model will be attempted, and higher resolution simulations will be undertaken to further elucidate the structure of the turbulence near the free surface.

## Acknowledgments

This work is supported by the Naval Research Laboratory under the Fluid Dynamics Task Area and the Office of Naval Research under the Surface Ship Wake Detection Program. Many of the calculations were performed under an NRL Cray Grant. The authors acknowledge the many fruitful discussions with J. D. Crouch.

## References

[1]Uzkan, T., and Reynolds, W., "A Shear-Free Turbulent Boundary Layer," *Journal of Fluid Mechanics,* Vol. 28, No. 4, 1967, pp. 803–821.

[2]Thomas, S. M., and Hancock, P. E., "Grid Turbulence Near a Moving Wall," *Journal of Fluid Mechanics,* Vol. 82, No. 3, 1977, pp. 481–496.

[3]Hunt, J., and Graham, J., "Free Stream Turbulence Near Plane Boundaries," *Journal of Fluid Mechanics,* Vol. 84, No. 2, 1978, pp. 209–235.

[4]Biringen, S., and Reynolds, W., "Large-Eddy Simulation of the Shear-Free Turbulent Boundary Layer," *Journal of Fluid Mechanics,* Vol. 103, Feb. 1981, pp. 53–63.

[5]Brumley, B., and Jirka, H., "Near-Surface Turbulence in a Grid Stirred Tank," *Journal of Fluid Mechanics,* Vol. 183, Oct. 1987, pp. 235–263.

[6]Orszag, S. A., and Patera, A. T., "Subcritical Transition to Turbulence in Planar Shear Flows," *Transition and Turbulence,* edited by R. E. Myer, Academic Press, London, 1981, pp. 127–146.

[7]Kim, J., Moin, P., and Moser, R., "Turbulence Statistics in a Fully Developed Channel Flow at Low Reynolds Number," *Journal of Fluid Mechanics,* Vol. 177, April 1987, pp. 133–136.

[8]Komori, S., Ueda, H., Ogino, F., and Mizushina, T., "Turbulence Structure and Transport Mechanism at the Free Surface in an Open Channel Flow," *International Journal of Heat and Mass Transfer,* Vol. 25, No. 4, 1982, pp. 513–521.

[9]Lam, K., and Banerjee, S., "On the Condition of Streak Formation in a Bounded Turbulent Flow," *Physics of Fluids A,* Vol. 4, No. 2, 1992, pp. 306–320.

[10]Nezu, I., and Rodi, W., "Open-Channel Flow Measurements with a Laser Doppler Anemometer," *ASCE Journal of Hydraulic Engineering,* Vol. 112, No. 5, 1986, pp. 335–355.

[11]Mansour, N. N., Moin, P., and Kim, J., "Reynolds-Stress and Dissipation Rate Budgets in a Turbulent Channel Flow," *Journal of Fluid Mechanics,* Vol. 194, Sept. 1988, pp. 15–44.

[12]Hanjalic, K., and Launder, B., "Contribution Towards a Reynolds-Stress Closure for Low-Reynolds Number Turbulence," *Journal of Fluid Mechanics,* Vol. 74, No. 4, 1976, pp. 593–610.

[13]Komori, S., Nagaosa, N., Murakami, Y., Chiba, S., Ishii, K., and Kuwahara, K., "Direct Numerical Simulation of Three-Dimensional Open Channel Flow with Zero-Shear Gas-Liquid Interface," *Physics of Fluids A,* Vol. 5, No. 2, 1993, pp. 115–125.

[14]Hossain, M., and Rodi, W., "Mathematical Modeling of Vertical Mixing in Stratified Channel Flow," *Proceedings, Second Symposium on Stratified Flows,* Trondheim, Norway, 1980.

[15]Naot, D., and Rodi, W., "Calculation of Secondary Currents in Channel Flow," *ASCE Journal of Hydraulic Engineering,* Vol. 108, No. HY8, 1982, pp. 948–968.

[16]Hinze, J. O., *Turbulence,* McGraw Hill, New York, 1975, Chap. 1.

[17]Swean, T. F., Jr., Leighton, R. I., Handler, R. A., and Swearingen, J. D., "Turbulence Modeling Near the Free Surface in and Open Channel Flow,"AIAA Paper 91-0613, 29th Aerospace Sciences Meeting, Reno, NV, Jan. 1991.

[18]Sirovich, L., "Turbulence Dynamics and Coherent Structures," *Quarterly of Applied Mathematics,* Vol. 45, No. 3, 1987, pp. 573–582.

[19]Kline, S., and Robinson, S., "Turbulent Boundary Layer Structure: Progress, Status and Challenges," *Proceedings of the 2nd International Union of Theoretical and Applied Mechanics Symposium on the Structure of Turbulence and Drag Reduction* (Zurich, Switzerland), Federal Inst. of Technology, 1989.

[20]Bernard, P., Thomas, J., and Handler, R., "Vortex Dynamics and the Production of Reynolds Stress," *Journal of Fluid Mechanics,* Vol. 253, Aug. 1993, pp. 385–419.

[21]Corrsin, S., *Symposium on Naval Hydrodynamics,* Publ. 515, Office of Naval Research, Washington DC, 1957, pp. 373–400.

[22]Kline, S. J., Reynolds, W. C., Schraub, J. A., and Runstadler, P. W., "The Structure of Turbulent Boundary Layers," *Journal of Fluid Mechanics,* Vol. 30, No. 4, 1967, pp. 741–773.

[23]Nakagawa, H., and Nezu, I., "Structure of Space-Time Correlations of Bursting Phenomena in an Open Channel Flow," *Journal of Fluid Mechanics,* Vol. 104, March 1981, pp. 1–43.

[24]Smith, C. R., and Metzler, S. P., "The Characteristics of Low-Speed Streaks in the Near-Wall Region of the Turbulent Boundary Layer," *Journal of Fluid Mechanics,* Vol. 129, April 1983, pp. 27–54.

[25]Schraub, F. A., and Kline, S. J., "A Study of the Structure of the Turbulent Boundary Layer with and Without Longitudinal Pressure Gradients," Dept. of Mechanical Engineering Rept. MD-12, Stanford Univ., Palo Alto, CA, 1965.

[26]Leighton, R. I., Swean, T. F., Jr., Handler, R. A., and Swearingen, J. D., "Interaction of Vorticity with a Free Surface in Turbulent Open Channel Flow," AIAA Paper 91-0236, 29th Aerospace Sciences Meeting, Reno, NV, Jan. 1991.